Hidden charm molecules in finite volume

M. Albaladejo[∗], **C. Hidalgo-Duque**[†], **J. Nieves, and E. Oset** [‡]

Instituto de Física Corpuscular (centro mixto CSIC-UV), Institutos de Investigación de Paterna, Aptdo. 22085, 46071, Valencia, Spain

April 5, 2013

Abstract

In the present paper we address the interaction of pairs of charmed mesons with hidden charm in a finite box. We use the interaction from a recent model based on heavy quark spin symmetry that predicts molecules of hidden charm in the infinite volume. The energy levels in the box are generated within this model, and from them some synthetic data are generated. These data are then employed to study the inverse problem of getting the energies of the bound states and phase shifts for $D\bar{D}$ or $D^*\bar{D}^*$. Different strategies are investigated using the lowest two levels for different values of the box size, carrying a study of the errors produced. Starting from the upper level, fits to the synthetic data are carried out to determine the scattering length and effective range plus the binding energy of the ground state. A similar strategy using the effective range formula is considered with a simultaneous fit to the two levels, one above and the other one below threshold. This method turns out to be more efficient than the other one. Finally, a method based on the fit to the data by means of a potential and a loop function conveniently regularized, turns out to be very efficient and allows to produce accurate results in the infinite volume starting from levels of the box with errors far larger than the uncertainties obtained in the final results. A regularization method based on Gaussian wave functions turns out to be rather efficient in the analysis and as a byproduct a practical and fast method to calculate the Lüscher function with high precision is presented.

1 Introduction

The determination of the hadron spectrum from lattice QCD (LQCD) calculations is attracting many efforts and one can get an overview on the different methods used and results in the recent review [1]. One of the tools becoming gradually more used is the analysis of lattice levels in terms of the Lüscher method [2,3]. This method converts binding energies of a hadron-hadron system in the finite box into phase shifts of hadron-hadron interaction from levels above threshold, or binding energies from levels below threshold [4–6]. From the phase shifts one can get resonance properties, and there are several works that have recently applied these techniques to study the ρ resonance [7–15]. There exist other resonances far more difficult to get with this approach like

[∗]Miguel.Albaladejo@ific.uv.es
[†]Carlos.Hidalgo@ific.uv.es
[‡]Eulogio.Oset@ific.uv.es

the $a_1(1260)$, which was also attempted in [14] (see also its determination using finite volume calculations with effective field theory in [16]). Scalar mesons have also been searched for with this method [17–20] and gradually some calculations are being performed for systems in the charm sector [21–27]. From another field theoretical perspective, finite volume calculations have also been devoted to this sector in [27–29]. In [28] the $\bar{K}D$, ηD_s interaction is studied in finite volume with the aim of learning about the nature of the $D_{s0}^*(2317)$ resonance from lattice data.[1] The theoretical model used in [28] is taken from [31], where the $D_{s0}^*(2317)$ resonance appears dynamically generated from the interaction of $\bar{K}D$, ηD_s and other less relevant channels. In this latter work, a scalar hidden charm state coming from the $D\bar{D}$ interaction with other coupled channels was also found, which qualifies basically as a $D\bar{D}$ quasi-bound state (decaying into pairs of lighter pseudoscalars). Although not reported experimentally, support for this state has been found in [32] from the analysis of the data of the $e^+e^- \to J/\psi D\bar{D}$ reaction of [33]. From the effective field theory point of view, this state has also been reported in [34, 35], using light SU(3)-flavour and heavy quark spin symmetries to describe charmed meson-antimeson interactions.

The purpose of the present paper is to study the interaction of $D\bar{D}$ and $D^*\bar{D}^*$ using a field theoretical approach in finite volume in order to evaluate energy levels in the finite box which might be compared with future LQCD calculations. The paper also presents a strategy to better analyze future lattice results in order to get the best information possible about bound states and phase shifts in the infinite volume case from these lattice data. For this purpose we shall use the model of [35], although most of the results and the basic conclusions are independent of which model is used.

As to the method to obtain the finite volume levels and the inverse problem of obtaining the results in the real world, phase shifts and binding energies, we shall follow the method of [36] where a reformulation of Lüscher approach is done based on the on shell factorization of the scattering matrix that one uses in the chiral unitary approach [37–42]. This method is conceptually and technically very easy and introduces improvements for the case of relativistic particles (although we shall not make use of the relativistic version in the present paper). Some works using this formalism can be found in Refs. [16, 28, 29, 43–47].

2 Formalism: infinite volume

In this section, we briefly review the formalism of Refs. [34, 35], where an effective field theory incorporating SU(3)-light flavour symmetry and heavy quark spin symmetry (HQSS) is formulated, to study charmed meson-antimeson (generically denoted here $H\bar{H}'$, with $H, H' = D, D^*, D_s, D_s^*$) bound states. The lowest order (LO) contribution of the interaction is given by contact terms, and the symmetries reduce the number of independent low energy constants (LECs) of the approach to only four. Other effects, like one-pion exchange or coupled channel dynamics, are shown to be sub-leading corrections to this order. Still, coupled channels will be considered explicitly when the mass difference between the thresholds is not negligible compared with the binding energy of the molecules considered. To fix the four constants of the approach, one assumes the molecular nature of some XYZ states, namely, $X(3872)$, $X(3915)$ and $Y(4140)$. The fourth input of the model is the isospin violating branching ratio

---

[1]The first hint, though indirect, of the nature of the $D_{s0}^*(2317)$ as a mostly $\bar{K}D$ bound state from lattice data was presented in [30]. There, lattice calculations of the scalar form factors in semileptonic pseudoscalar-to-pseudoscalar decays were used to extract information about the corresponding elastic S-wave scattering channels.

of the decays $X(3872) \to J/\Psi\omega$ and $X(3872) \to J/\Psi\rho$ (for a different approach to this issue and the $X(3872) \to J/\Psi\gamma$ decay see [48]). For further details on the formalism we refer to Refs. [34, 35, 49]. We will adapt here the formalism to a more adequate (for the problem in hands) T-matrix language.

Since we are dealing with heavy mesons, we use a non-relativistic formalism. In our normalization, the S-matrix[2] for an elastic $H\bar{H}'$ scattering process reads

$$S(E) \equiv e^{2i\delta(E)} = 1 - i\frac{\mu k}{\pi}T(E) \ , \tag{2.1}$$

where the modulus of the momentum $k = |\vec{k}|$ is given by $k^2 = 2\mu(E - m_1 - m_2)$, and μ is the reduced mass of the system of two particles with masses m_1 and m_2. In Eq. (2.1), δ is the phase shift, and we can write:

$$T = -\frac{2\pi}{\mu k}\sin\delta e^{i\delta} \ , \tag{2.2}$$

$$T^{-1} = -\frac{\mu k}{2\pi}\cot\delta + i\frac{\mu k}{2\pi} \ . \tag{2.3}$$

The expression for the T-matrix is given by:

$$T^{-1}(E) = V^{-1}(E) - G(E) \ , \tag{2.4}$$

with V the potential (two-particle irreducible amplitude) and G a one-loop two-point function. This equation stems from a once-subtracted dispersive representation of $T^{-1}(E)$ (see for instance Sec. 6 of Ref. [39]), or equivalently, from the N/D method [50] equations, when the left-hand cut is neglected or included perturbatively [40, 51–53]. The loop function G provides the right-hand cut and the contribution of the left-hand cut should be included in the potential V. As mentioned above, we will follow here the approach of Refs. [34, 35], and we will approximate V by its LO contribution in the $1/m_Q$ expansion (with m_Q the mass of the heavy quark). Thus, we are completely neglecting the left-hand cut.

The loop function G needs to be regularized in some way. Typical approaches are once-subtracted dispersion relations and sharp cutoffs. Here, instead, we are following the approach of Refs. [34, 35], in which the loop function is regularized with a Gaussian regulator. For an arbitrary energy E, we find

$$\begin{aligned} G(E) &= \int \frac{\mathrm{d}^3\vec{q}}{(2\pi)^3} \frac{e^{-2(\vec{q}^2 - k^2)/\Lambda^2}}{E - m_1 - m_2 - \vec{q}^2/2\mu + i0^+} \\ &= -\frac{\mu\Lambda}{(2\pi)^{3/2}}e^{2k^2/\Lambda^2} + \frac{\mu k}{\pi^{3/2}}\phi\left(\sqrt{2}k/\Lambda\right) - i\frac{\mu k}{2\pi} \ , \end{aligned} \tag{2.5}$$

with $\phi(x)$ given by:

$$\phi(x) = \int_0^x e^{y^2}\mathrm{d}y \ . \tag{2.6}$$

Note that, the wave number k is a multivalued function of E, with a branch point at threshold ($E = m_1 + m_2$). The principal argument of $(E - m_1 - m_2)$ should be taken in the range $[0, 2\pi[$. The function $k\phi(\sqrt{2}k/\Lambda)$ does not present any discontinuity for real E above threshold, and

---

[2]We will always consider $S-$wave meson-antimeson interactions, and thus the spin of the molecule will always coincide with the total spin of the meson-antimeson pair. The partial waves $^{2S+1}L_J$ are then $^{2S+1}S_{J=S}$. For simplicity in what follows, we will drop all references to the L, S and J quantum numbers, both in the S and T matrices.

$G(E)$ becomes a multivalued function because of the ik term. Indeed, $G(E)$ has two Riemann sheets. In the first one, $0 \leqslant \text{Arg}(E - m_1 - m_2) < 2\pi$, we find a discontinuity $G_I(E + i\epsilon) - G_I(E - i\epsilon) = 2i \, \text{Im} G_I(E + i\epsilon)$ for $E > (m_1 + m_2)$. It guaranties that the T−matrix fulfills the optical theorem. For real values of E and below threshold, we have $k = i\sqrt{-2\mu(E - m_1 - m_2)}$. Poles below threshold in the first sheet correspond to bound states. In the second Riemann sheet, $2\pi \leqslant \text{Arg}(E - m_1 - m_2) < 4\pi$, we trivially find $G_{II}(E - i\epsilon) = G_I(E + i\epsilon)$, for real energies and above threshold.

The Gaussian form factor enters Eq. (2.5) in a way that is unity for on-shell momenta, and hence the optical theorem $\text{Im} T^{-1} = \mu k/(2\pi)$ is automatically fulfilled. A Gaussian regulator is also used in Ref. [54] to study the Δ resonance in finite volume.

The cutoff Λ is a parameter of the approach, and, hence, the theory depends on it. This dependence, however, is partially reabsorbed in the counter-terms of the theory, as long as one chooses a reasonable value for it, not beyond the high-energy scale of the effective field theory [55–58].

In the approach of Refs. [34, 35], the potential V is taken as

$$V(E) = e^{-2k^2/\Lambda^2} C(\Lambda) \,, \tag{2.7}$$

where C is the proper combination of the four different counter-terms for each considered channel $H\bar{H}'$. Explicit expressions can be found in Appendix A. The dependence of the counter-term on the ultraviolet (UV) cutoff Λ should cancel that of the loop function G, such that $G(E_B)V(E_B)$ becomes independent of Λ, when E_B is the energy of the bound state used to determine the counter-term.[3] For other energies, there will exist a remaining, unwanted/unphysical, dependence of the T matrix on the cutoff. This is due to the truncation of the perturbative expansion (see discussion in Ref. [34]). Up to this point, we have discussed only the case of uncoupled channels, but the generalization to coupled channels is straightforward.[4]

Finally, above threshold the effective range expansion reads:

$$k \cot \delta = -\frac{1}{a} + \frac{1}{2} r k^2 + \cdots \,, \tag{2.8}$$

where a and r are, respectively, the scattering length and the effective range. From Eqs. (2.3) and (2.4) we can calculate the theoretical predictions for these effective range parameters, obtaining:

$$a_{\text{th}} = \frac{\mu}{2\pi} \left(\frac{1}{C} + \frac{\mu\Lambda}{(2\pi)^{3/2}} \right)^{-1} \,, \tag{2.9}$$

$$r_{\text{th}} = -\frac{8\pi}{\mu\Lambda^2} \left(\frac{1}{C} - \frac{\mu\Lambda}{(2\pi)^{3/2}} \right) . \tag{2.10}$$

3 Formalism: finite volume

In this section, we follow the steps of Ref. [36] to write the amplitude in a finite box of size L with periodic boundary conditions, denoted by $\tilde{T}$. Since the potential does not depend on

---

[3]The mass of a bound state is thus given by $T^{-1}(E_B) = 0$ for $E_B < m_1 + m_2$, which is the equivalent of Eq. (10) in Ref. [35].

[4]One just has to rewrite the T-matrix as $T = (\mathbb{I} - VG)^{-1}V$, where V and G are now matrices in the coupled channels space.

L, one only has to replace the loop function G with its finite volume version, $\tilde{G}$, in which the integral over momentum $\vec{q}$ is replaced by a discrete sum over the allowed momenta,

$$\tilde{T}^{-1}(E) = V^{-1}(E) - \tilde{G}(E) \; , \tag{3.1}$$

$$\tilde{G}(E) = \frac{1}{L^3} \sum_{\vec{q}} \frac{e^{-2(\vec{q}^2 - k^2)/\Lambda^2}}{E - m_1 - m_2 - \vec{q}^2/2\mu} \; , \tag{3.2}$$

where the (quantized) momentum is given by:

$$\vec{q} = \frac{2\pi}{L}\vec{n} \; , \quad \vec{n} \in \mathbb{Z}^3 \; . \tag{3.3}$$

Now, the energy levels in the box are given by the poles of the $\tilde{T}$-matrix, $V^{-1} = \tilde{G}$. For the energies of these levels in the box, the amplitude in the infinite volume is recovered as:

$$T^{-1}(E) = V^{-1}(E) - G(E) = \tilde{G}(E) - G(E) = \delta G(E) \; . \tag{3.4}$$

Since the G function is regularized (either in the box or in the infinite volume) with a Gaussian regulator, the difference above depends explicitly on the cutoff Λ. This remaining non-physical dependence on Λ quickly disappears as the volume increases. Indeed, we find that it is exponentially suppressed and that it dies off as $\exp{(-L^2\Lambda^2/8)}$ (see Appendix B). Thus, it is clear that in this context, we can end up the renormalization program just by sending the UV cutoff to infinity. This will allow to obtain the physical $T-$matrix, independent of any renormalization scale, for the energy levels found in the lattice Monte Carlo simulation (finite box).

For the practical calculations that we will show in what follows, the Λ dependence is already negligible when $\Lambda \gtrsim 1$ GeV even for the smallest volumes considered in this work (the limit $\Lambda \to \infty$ is effectively achieved for such values). In this limit, Eq. (3.4) becomes the Lüscher equation [2, 3], as we discuss in certain detail in Appendix B. The results of the appendix also show that the inclusion of a Gaussian regulator is a quite efficient technique, from the computational point of view, to evaluate the Lüscher function $\mathcal{Z}_{00}(1, \hat{k}^2)$ used in [3]. Finally, from Eqs. (2.3) and (3.4), we can write:

$$k\cot\delta = -\frac{2\pi}{\mu} \lim_{\Lambda \to \infty} \text{Re}\left(\tilde{G}(E) - G(E)\right) \; . \tag{3.5}$$

4 Results

We present in this section the results obtained with the formalism outlined in the previous section. We first discuss the results obtained by putting the model of Refs. [34, 35] directly in the box. That is, we study the volume dependence of the molecules found in Ref. [35], predicting thus the existence of sub-threshold levels (asymptotically different of threshold) for the different channels, which have a clear correspondence with the hidden charm molecules reported in [35]. This is done in Subsec. 4.1.

Our purpose in Subsecs. 4.2, 4.3 and 4.4 is to simulate a realistic situation in a LQCD study, where one would obtain different energy levels (one or two) for different sizes, L, of the box. To do so, we generate "synthetic data" from the exact levels that we obtain from the model of Refs. [34, 35]. We take five different values of L_i, in the range $Lm_\pi = 1.5$ to 3.5. From the calculated levels, we obtain randomly shifted levels (in a range of 5 MeV), and assign an error of 10 MeV to each of these points, except the last one for which we have assumed an error of

only 8 MeV to prevent it from crossing the threshold. Next we use a Monte Carlo simulation, to estimate the errors on the determination of observables (the phase shifts, for instance) when the energy levels are obtained with a certain statistical error. Specifically, we study in these subsections the $I = 0$ $J^{PC} = 0^{++}$ $D\bar{D}$ channel.

In Subsec. 4.2, the Lüscher formalism to study the phase shifts calculated from Eq. (3.5) is applied to the synthetic levels above threshold that we find for the different studied channels. From these phase shifts, we calculate the effective range expansion parameters, and use them to determine the masses of the bound states. In Subsec. 4.3 we adopt another strategy to extract information from the generated levels. Namely, we consider a potential which parameters are then fitted to reproduce the synthetic levels (above and below threshold, simultaneously). With this potential, we can make predictions in the infinite volume case, and thus we end up with another determination of the masses of the predicted bound states. We shall see that this method allows one to obtain better results (better central value and smaller errors) for the mass of the bound state than the previous one. We then analyze in detail which are the differences of both approaches. In Subsec. 4.4 another method is proposed, in which the effective range approximation is retained for the inverse of the T-matrix amplitude, but fitting directly the energy levels instead of the phase shifts, and studying simultaneously the levels above and below threshold. In this case, then, we notice that the precision achieved for the mass of the bound state is similar to that obtained with the potential analysis.

In Subsec. 4.5, we analyze in a more quantitative way, the qualitative arguments given in Subsec. 4.1, where the behavior of the sub-threshold levels is discussed. We offer a method to discriminate between those levels that produce bound states in the limit $L \to \infty$ and those that do not, and hence tend to threshold in the infinite volume limit. This method allows the extraction of the mass and the coupling of the bound state in the infinite volume limit.

All these methods are applied in Subsec. 4.6 to the bound state present in the $I = 0$ $J^{PC} = 2^{++}$ $D^*\bar{D}^*$ channel. The difference with respect to the case used as an example in the previous subsections is that the state is now weakly bound (the binding energy is only around 2–3 MeV), so that we can compare how the methods exposed above work for this case.

4.1 The model of Ref. [35] in a finite box

In Figs. 1 and 2 we present the dependence of the energy levels on the size of the finite box, as calculated from Eqs. (3.1) and (3.2), for the different channels studied in Ref. [35]. We have fixed the potential in the different channels by means of the central values given in this reference for the various counter-terms, and collected here in Appendix A, Eqs. (A.3)–(A.6). When needed, we have also implemented in the finite box a coupled channel formalism. The solid lines correspond to the case $\Lambda = 1$ GeV, whereas the dot-dashed lines to $\Lambda = 0.5$ GeV. For comparison, we also show, with the horizontal dashed lines, the involved threshold energies. We just show those energy levels that can be identified with bound states ($k^2 < 0$) in the infinite volume case. That is, their asymptotic $L \to \infty$ value approaches the bound energies given in [35], and thus they are different from threshold. Of course, one has this latter piece of information from the calculations of the model in an infinite volume, but this would not be the case in a lattice simulation. Let us focus, for simplicity, in the $I = 0$ case, shown in the left panel of Fig. 1. The large L asymptotic behavior can be well appreciated in some cases like the 0^{++} $D\bar{D}$ or 1^{+-} $D^*\bar{D}$ molecules. However in other cases, it might be difficult to discriminate between a real bound state and a threshold level, even for quite large values of the box size L. Clear examples are the 1^{++} $D^*\bar{D}$ or the 2^{++} $D^*\bar{D}^*$ molecules (similar examples can be found in
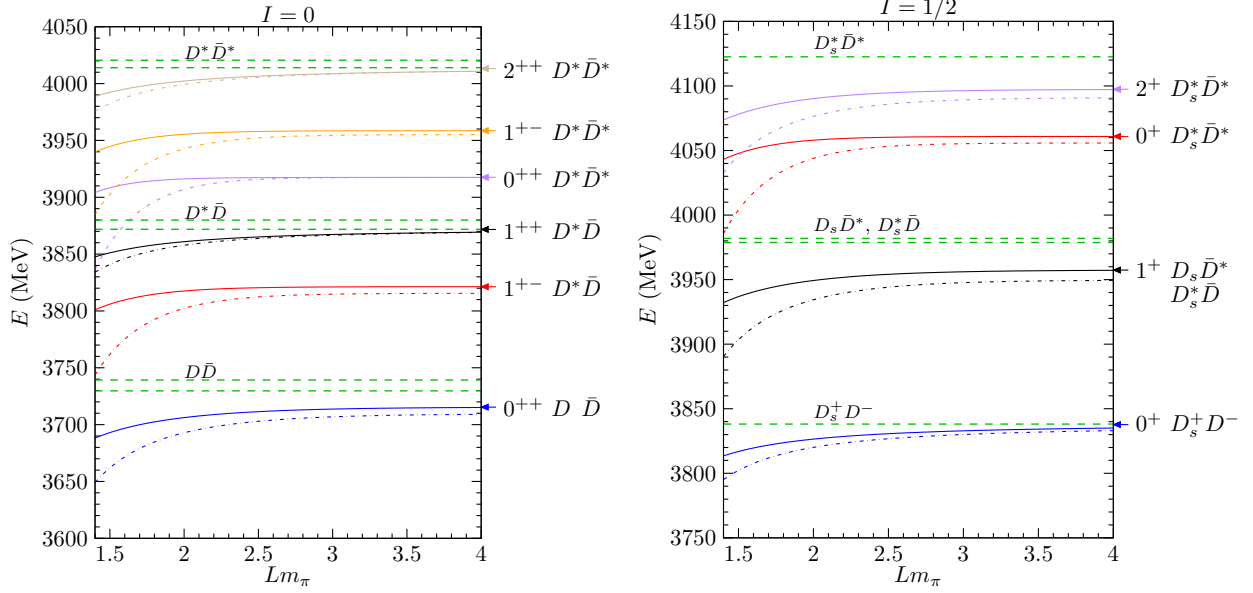
Figure 1: Volume dependence of the $I = 0$ (left) and $I = 1/2$ (right) molecules predicted in Ref. [35]. The horizontal dashed lines show the different thresholds involved (when the charge is not explicitly given, we are displaying the thresholds associated to the different charge channels). The solid lines correspond to the levels found in the box for $\Lambda = 1$ GeV, whereas the dot-dashed ones stand for those obtained with $\Lambda = 0.5$ GeV. Over the right axis we mark with arrows the masses of the bound states as predicted in the infinite volume case and $\Lambda = 1$ GeV. The J^{PC} quantum numbers of the different channels are indicated beside the arrows.

the different isospin-strangeness channels), which in the infinite volume case are loosely bound.[5] Thus, we see a well known result from Quantum Mechanics; the smaller the binding energies, the larger become the L values needed to reach the asymptotic behavior. From this study, we conclude that in a lattice simulation when dealing with states that are at least bound by some tens of MeV, one might safely discriminate them by using box sizes of the order of $Lm_\pi \simeq 3$. However, the lattice study of other states less bound (binding energies below 4 or 5 MeV, as in the case of the $X(3872)$ or the 2^{++} resonances) might require significantly larger volumes. To achieve more accurate predictions for the former and solve the problem for the latter ones, we follow different approaches in the following subsections.

Finally, we note that some of the levels in Figs. 1 and 2 are not realistic, in the sense that they would mix with other levels generated by channels with the same quantum numbers, but lower thresholds. That is the case, for example in $I = 0$, of the 0^{++} $D^*\bar{D}^*$ at $E \simeq 3920$ MeV, that would mix with some higher levels of the $D\bar{D}$ channel. Indeed, it is to be expected that these bound states would acquire some width due to the coupled channel dynamics. Still, it is possible that these states could appear as more or less stable energy levels.[6]

---

[5]The first one corresponds to the $X(3872)$ resonance that has been observed close to the $D^0\bar{D}^{0*}$ threshold [59] (see also a recent determination and discussion of other experiments in Ref. [60]) and it has been a hot topic for both the experimental and theory communities since its discovery. The 2^{++} state is a HQSS partner of the $X(3872)$ molecule which dynamics, at LO in the heavy quark expansion, is being determined by precisely the same combination of counter-terms that appear in the $X(3872)$ channel. Given the discovery of the $X(3872)$ resonance, the existence of the 2^{++} state, either as a bound state or a resonance, is therefore a quite robust consequence of HQSS [34, 35].

[6]In Ref. [61] the $D^*\bar{D}^*$, $D_s^*\bar{D}_s^*$ states are studied with the interaction taken from the extrapolation of the local hidden gauge approach to the charm sector, which also respects HQSS. The coupling to $D\bar{D}$ and $D_s\bar{D}_s$ is allowed and generates a width of about 50 MeV for the most bound state, the one with $I = 0$ and $J^{PC} = 2^{++}$.
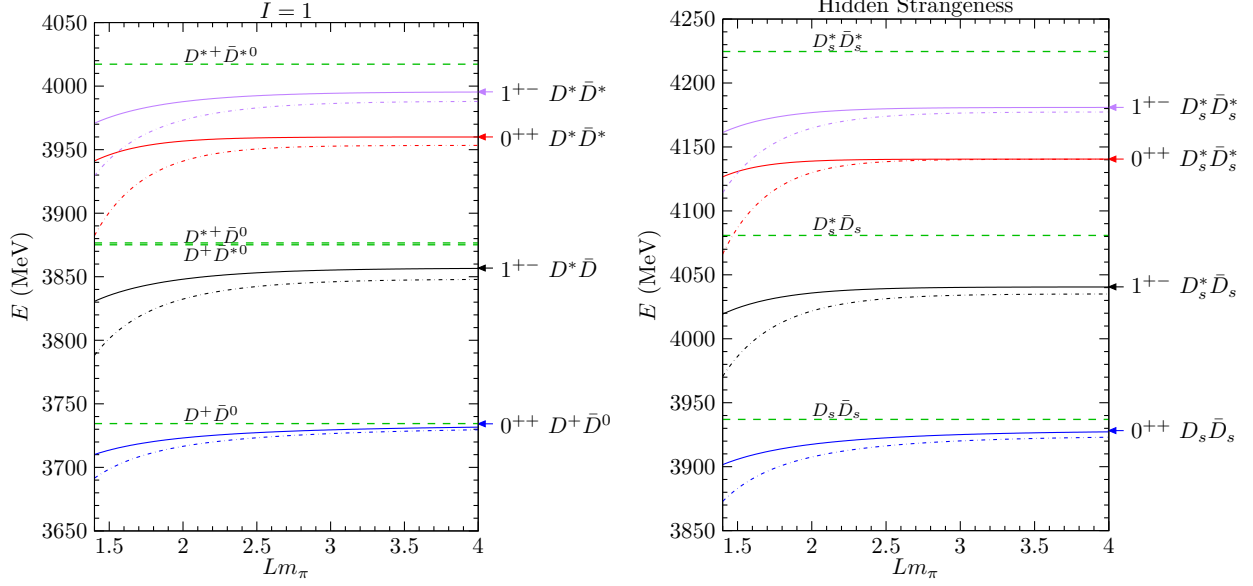
Figure 2: The same as in Fig. 1 for the $I = 1$ (left) and hidden strangeness (right) molecules predicted in Ref. [35].

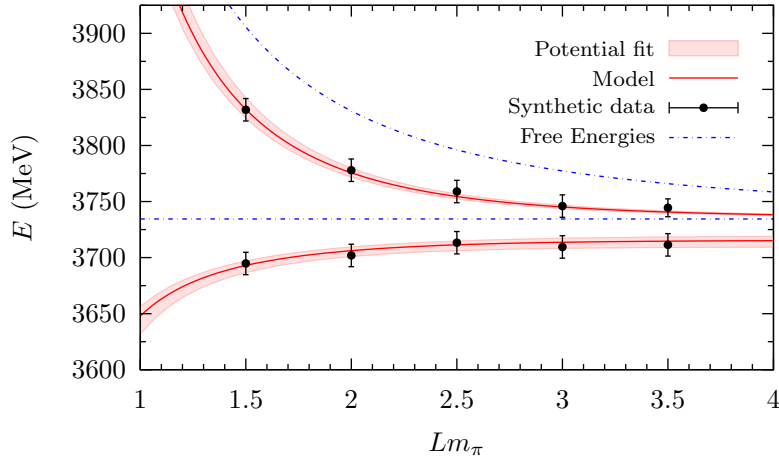## 4.2 Inverse analysis: phase shifts

Figure 3: Some energy levels for the $I = 0$, $J^{PC} = 0^{++}$ $D\bar{D}$ interaction as a function of the box size L. The levels obtained with the model of Refs. [34,35] in a box for $\Lambda = 1$ GeV are shown with (red) solid lines, while the generated levels for some particular values of L (synthetic data points, see the text for details), together with their assigned errors are displayed with black circles. The non-interacting energies $(m_1 + m_2 + (2\pi/L)^2 n^2/2\mu$ with $n = 0, 1)$ are shown with (blue) dash-dotted lines. The error bands around the solid lines are obtained from the fit to a potential discussed in Subsec. 4.3. They have been obtained by considering pairs of fitted parameters $(1/C_{0a}, \Lambda)$ that provide values of χ^2 that differ from the minimum one by less than one unit $(\chi^2 \leqslant \chi^2_{\min} + 1)$.

We start discussing the case of the isoscalar 0^{++} $D\bar{D}$ interaction. Some levels found from the model of Ref. [35] in a finite box,[7] obtained as the zeros of Eq. (3.1), are shown with a (red) solid line in Fig. 3. The synthetic levels generated from them and our choice for their errors are shown with points. Recall that we give an error of ± 10 MeV to these points trying to simulate a realistic situation in a LQCD study, where these levels will be determined with

---

[7]In what follows we will use an UV cutoff $\Lambda = 1$ GeV when presenting results deduced from the model of Ref. [35], both for finite boxes and in the infinite volume case. Other cutoffs compatible with the effective theory designed in [34,35] give rise to similar results.
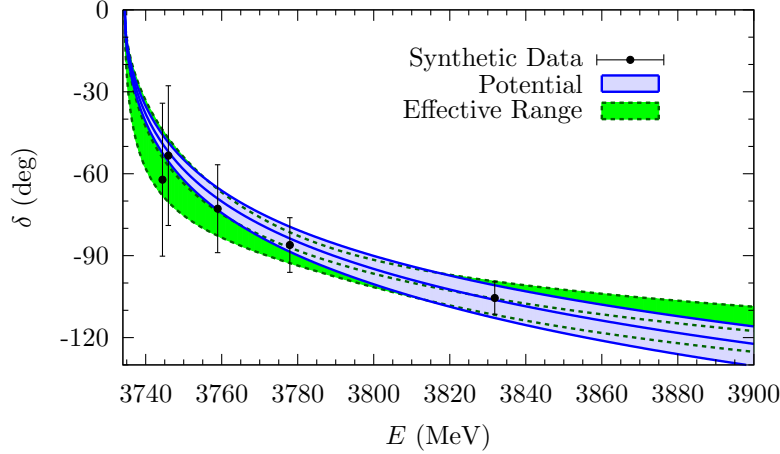
Figure 4: Phase shifts obtained for $I = 0$ $J^{PC} = 0^{++}$ $D\bar{D}$ interaction. The points stand for the phase shifts calculated from the synthetic energy levels displayed in Fig. 3 using Eq. (3.5). The green dashed line and its associated error band corresponds to the effective range analysis of Subsec. 4.2, while the blue solid line and its error band stand for the results obtained by fitting a potential discussed in Subsec. 4.3. The phase shifts in the infinite volume are very similar to the latter ones, so we do not show them. In both cases, the error bands have been obtained by considering pairs of fitted parameters $[(1/a, r)$ for the effective range fit and $(1/C_{0a}, \Lambda)$ for the case of the potential fit] that provide values of χ^2 that differ from the minimum one by less than one unit (points included in the dark blue $\chi^2 \leqslant \chi^2_{\min} + 1$ ellipse displayed in Fig. 5).

some statistical uncertainties. From the upper level and the Lüscher's formula, Eq. (3.5), we find the phase shifts shown with points in Fig. 4. The errors in the phase shifts in this figure are determined by recalculating them, through Eq. (3.5), with different values of the upper level energy, E, randomly taken within the error intervals displayed for each of the synthetic data points in Fig. 3.

We could also obtain the scattering length and the effective range parameters either from the determined phase shifts, or from Eqs. (2.8) and (3.5). Actually, combining these two latter equations we have,

$$\operatorname{Re} \delta G_L = \lim_{\Lambda \to \infty} \operatorname{Re}\left(\tilde{G}(E) - G(E)\right) = -\frac{2\pi}{\mu}\left(-\frac{1}{a} + \frac{1}{2}rk^2 + \cdots\right) \tag{4.1}$$

for the upper energy levels, E, determined in finite boxes of different sizes. We have obtained $1/a$ and r from a χ^2−linear fit to the five data points generated for $\operatorname{Re} \delta G_L$ using the five synthetic upper energy levels[8] shown in Fig. 3. We find

$$\frac{1}{a} = 0.62 \pm 0.25 \text{ fm}^{-1}, \qquad r = 0.53 \pm 0.18 \text{ fm} \tag{4.2}$$

with a linear Gaussian correlation coefficient $R = 0.83$. From the above result, we find

$$a = 1.6^{+1.0}_{-0.5} \text{ fm} . \tag{4.3}$$

These values are to be compared with those obtained in the infinite volume model, Eqs. (2.9) and (2.10), with parameter $C = C_{0a}(\Lambda = 1 \text{ GeV}) = -1.024 \text{ fm}^2$, which turn out to be:

$$a_{\text{th}} = 1.38 \text{ fm} , \quad r_{\text{th}} = 0.52 \text{ fm} . \tag{4.4}$$

---

[8]To estimate the errors in $\operatorname{Re} \delta G_L$ for each of the synthetic energy levels considered, we follow a procedure similar to that outlined above for the phase shifts. Thus, we let the synthetic energy level vary within the error interval displayed in Fig. 3 and find the range of variation of $\operatorname{Re} \delta G_L$.

9

Our fitted values are compatible with the theoretical ones, but have sizeable errors, although the correlation is large. Performing a standard analytical continuation of Eqs. (2.3) and (2.8) below the $D\bar{D}$ threshold, we estimate the position of the $X(3715)$ bound state,

$$E = 3721^{+10}_{-25} \text{ MeV} , \tag{4.5}$$

whereas the value found in Ref. [35] is $E = 3715^{+12}_{-15}$ MeV.[9] The binding energy, $B < 0$, is obtained from Eqs. (2.3) and (2.8), upon changing $k \to i\kappa$, and imposing $T^{-1} = 0$,

$$B = \frac{\kappa^2}{2\mu} , \qquad \kappa = \frac{1 \pm \sqrt{1 - 2r/a}}{r} . \tag{4.6}$$

To estimate the uncertainties in Eq. (4.5), we have performed a Monte Carlo simulation taking into account the existing statistical correlations between $1/a$ and r. We quote a 68% confident interval (CL), but with some caveats as we explain next. Note that $2r/a$ is not far from unity and within errors it can be even bigger, which means that we can get some events in the Monte Carlo runs (around 25%) with $1 - 2r/a < 0$, for which we set the square root to zero. Thus, the lower error quoted in Eq. (4.5) is somehow uncertain, since the above procedure tends to accumulate events around 3695 MeV. On the other hand, for the cases with $1 - 2r/a > 0$, but small, the two roots of κ in Eq. (4.6) are not so different, and hence there is some ambiguity in the binding energy B (we choose the smallest value of κ). Note that, although the value of E obtained with its errors seems quite accurate, when one considers it relative to the binding energy B, we find a large dispersion, since the $D\bar{D}$ threshold is at around 3734 MeV.

Finally, if we decrease the error of the synthetic energy levels from 10 MeV to 5 MeV, then the errors of the phase shifts as well as those of the threshold parameters are also reduced approximately to half of their previous values, and the predicted mass is more accurate, $E = 3723^{+5}_{-11}$ MeV (and now only for around 6% of the Monte Carlo events, $1-2r/a$ become negative). This should give an idea of the precision needed in the determination of the energy levels in order to have an appropriate determination of the mass.

In the next sections we discuss different alternatives that allow to achieve a better precision.

4.3 Inverse analysis: fit to a potential

We now consider another approach to analyze/use the synthetic levels that we generated in the previous section. Here again we aim to falsifying real data obtained from LQCD Monte Carlo simulations for various finite volumes. The analysis of phase shifts in the previous subsection necessarily takes into account only the level above threshold in Fig. 3. It is then convenient to develop an approach that could simultaneously make use of all available levels. Thus, we propose to describe all levels using a potential, Eqs. (2.7) and (3.1), fitting its parameters for such purpose. We adopt here an approach where we fit a counter-term $C = C_{0a}$ defining the potential[10] and the UV cutoff Λ (involved in the finite box loop function and in the potential (see Eq. (2.7)) to the synthetic energy levels shown in Fig. 3. Thus, the χ^2 function is then given by:

$$\chi^2 = \sum_{i=1}^{5} \frac{\left(E_{\text{thV}}^{(0)}(L_i) - E_i^{(0)}\right)^2}{\left(\Delta E_i^{(0)}\right)^2} + \sum_{i=1}^{5} \frac{\left(E_{\text{thV}}^{(1)}(L_i) - E_i^{(1)}\right)^2}{\left(\Delta E_i^{(1)}\right)^2} , \tag{4.7}$$

[9]The errors calculated for finite volume quantities in this work refer to the statistical uncertainties we generate in the synthetic data. The errors quoted from Ref. [35] refer instead to the uncertainties in the determination of the constants appearing in the potential.

[10]We follow here the notation of [34, 35] where the counter-term that appears in this channel is called C_{0a} (see Appendix A).

where $E_{\text{thV}}^{(0,1)}(L_i)$ are the first two energy levels calculated from the HQSS potential, with parameters C_{0a} and Λ, in a finite box of size L_i. On the other hand, $E_i^{(0,1)}$ and $\Delta E_i^{(0,1)}$ are the synthetic levels, that we have generated, together with their assigned errors. Here, the superscript $j = 0, 1$ refers to the two levels shown in Fig. 3. The fit parameters, $1/C_{0a}$ and Λ, obtained in the best fit are

$$\frac{1}{C_{0a}} = -0.93 \pm 0.20 \text{ fm}^{-2}, \qquad \Lambda = 970 \pm 130 \text{ MeV} , \qquad (4.8)$$

with a linear Gaussian correlation coefficient $R = -0.98$. These errors, and the correlation coefficient, are calculated from the hessian of χ^2 at the minimum. However, since the fit is not linear, these errors are slightly different from those obtained requiring $\chi^2 \leqslant \chi_{\text{min}}^2 + 1$. This latter requirement gives the following non-symmetrical errors:

$$\frac{1}{C_{0a}} = -0.93_{-0.27}^{+0.18} \text{ fm}^{-2}, \qquad \Lambda = 970_{-120}^{+180} \text{ MeV} , \; . \qquad (4.9)$$

From Eq. (4.8), we find $C_{0a} = -1.08_{-0.29}^{+0.19} \text{ fm}^2$. The central values of both, the counter-term and the UV cutoff, agree well with those of the original model of Ref. [35], $C_{0a} = -1.024 \text{ fm}^2$ and $\Lambda = 1$ GeV, used to generate the synthetic levels. However, as expected, the two parameters are strongly correlated. This is further discussed in Appendix C. A contour plot of the χ^2 function in the $(1/C_{0a}, \Lambda)$−plane is shown in Fig. 5, that manifestly shows the correlation.

On the other hand, the fitted parameters of Eq. (4.8) predict a value for the mass of the bound state of $E = 3715_{-6}^{+3}$ MeV (68% CL, obtained from a Monte Carlo Gaussian simulation keeping the statistical correlations) in the infinite volume case. The central value agrees remarkably well with the value obtained from the model of Ref. [35], $E = 3715$ MeV, and certainly much better than that obtained with the phase shift analysis carried out in the previous subsection ($E = 3721_{-25}^{+10}$ MeV). The errors found now are also significantly smaller.

Finally, we have calculated error bands for the predicted finite box levels and phase shifts by quantifying the variations that are produced in these observables when one randomly considers pairs $(1/C_{0a}, \Lambda)$ of parameters that provide $\chi^2 \leqslant \chi_{\text{min}}^2 + 1$ (points included in the dark blue ellipse displayed in Fig. 5). These error bands are shown in Figs. 3 and 4, respectively.
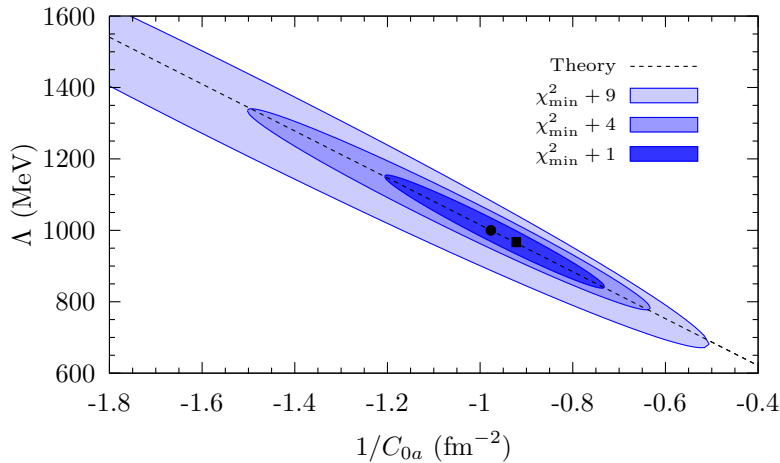

Figure 5: Contour plots for the χ^2 function defined in Eq. (4.7) for the $I = 0$ $J^{PC} = 0^{++}$ $D\bar{D}$ channel. The dashed line shows the correlation predicted from the model of Ref. [35], Eq. (C.2). The circle represents the central value taken for that model, $C_{0a} = -1.024 \text{ fm}^2$ and $\Lambda = 1$ GeV, while the square stands for the results of the best fit of Eq. (4.8).

11

4.4 Inverse analysis: effective range

We have seen in Subsecs. 4.2 and 4.3 that the fit of the synthetic energy levels with a potential leads to better results for the mass of the bound state than those obtained from the fit to the phase shifts (deduced from the upper level) with the effective range expansion. We believe that the reasons for this improvement are basically three. First, the potential fit takes into account both levels, above and below threshold, while the phase shifts analysis takes into account just the upper level. Second, in the potential fit, the "observables" are the energy levels, while, in the phase shifts analysis, the quantity that enters in the χ^2 function is $k \cot \delta$, and the propagation of errors can lead thus to worse determinations of the parameters. Third, the analytical structure of the inverse of the amplitude is different in both approaches. In the effective range approach, ones truncates a series up to k^2, while in the potential fit one is effectively including further terms beyond the latter ones. Indeed, the full loop function G is taken into account. To study the importance of the first two points, we follow here another approach, in which we shall keep the effective range approximation for the amplitude, but fit the energy levels (above and below threshold) instead of the phase shifts obtained from the above threshold level.

The effective range expansion for the inverse of the T-matrix is written from Eqs. (2.3) and (2.8):

$$T^{-1}(E) = \begin{cases} -\frac{\mu}{2\pi}\left(-\frac{1}{a} + \frac{r}{2}k^2 - ik\right) , & k = \sqrt{2\mu(E - m_1 - m_2)} , \ E > m_1 + m_2 \\ -\frac{\mu}{2\pi}\left(-\frac{1}{a} - \frac{r}{2}\gamma^2 + \gamma\right) , & \gamma = \sqrt{2\mu(m_1 + m_2 - E)} , \ E < m_1 + m_2 \end{cases} . \quad (4.10)$$

Now, the energy levels in the box are found for given values of a and r, by means of Eq. (3.4). It is to say, by numerically solving $T^{-1}(E) = \delta G_L(E)$, similarly as it is done in the case of the potential, but now using Eq. (4.10) to model the $T-$matrix both above and below threshold. We will denote the levels obtained in this manner as $E_{\text{thEF}}^{(j)}$. To determine the best values of a and r, we consider thus a χ^2 function as Eq. (4.7), where the $E_i^{(j)}$ are still the synthetic levels we have generated, but replacing the $E_{\text{thV}}^{(j)}$ by $E_{\text{thEF}}^{(j)}$, calculated as explained above. The values of the best parameters are:

$$\frac{1}{a} = 0.70 \pm 0.07 \text{ fm}^{-1}, \qquad r = 0.56 \pm 0.07 \text{ fm} , \quad (4.11)$$

with a linear Gaussian correlation coefficient $R = -0.6$.[11] Hence, we obtain:

$$a = 1.43^{+0.16}_{-0.13} \text{ fm} . \quad (4.12)$$

The errors calculated in this way are clearly smaller than those displayed in Eq. (4.2) with the phase shifts analysis carried out in Subsec. 4.2. Also, the central value of the scattering length agrees better with the theoretical one, Eq. (4.4). These improvements have a clear impact in the determination of the mass of the bound state, which is now $E_B = 3716^{+4}_{-5}$ MeV (68% CL), with smaller errors and better central value than those obtained with the phase shifts analysis in Eq. (4.5). In Fig. 6 we show a comparison of the ellipses in the $(1/a, r)$ parameter space determined by the condition $\chi^2 \leqslant \chi^2_{\min} + 1$ for the fits of Eqs. (4.2) and (4.11). There, it can be clearly appreciated the significant improvement achieved by fitting directly to both, lower and upper energy levels, instead of fitting to the phase shifts deduced from the latter levels. Finally, we must point out that the determination of the energy levels obtained with this method are very similar to those obtained in Subsec. 4.3 by introducing of a potential, and shown in Fig. 3.

---

[11]In this case, the errors calculated from the requirement $\chi^2 \leqslant \chi^2_{\min} + 1$ almost coincided with those given here in Eq. (4.11).
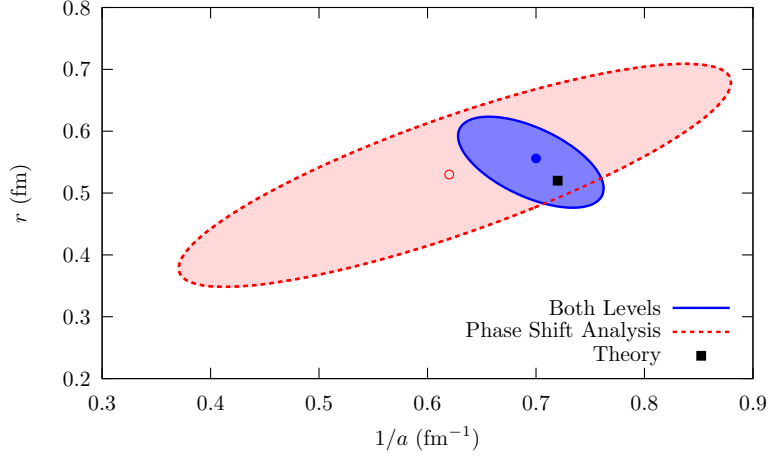
Figure 6: Comparison of the determination of the effective range parameters, $1/a$ and r, with the methods explained in Subsecs. 4.2 (red dashed line) and 4.4 (solid blue line). The ellipses are obtained from the condition $\chi^2 \leqslant \chi^2_{\min} + 1$ in each case. The central values of each fit are represented with points. We also show, for comparison, the theoretical values of the parameters, as given in Eq. (4.4), with a black square.

Actually, the differences between the upper and lower energy level curves (and their error bands) deduced from both methods would not be easily appreciated in Fig. 3. For this reason, we have not shown in this figure the results obtained from the method discussed in this subsection.

4.5 Inverse analysis: bound state fit

We have discussed in Subsec. 4.1 the volume dependence of the sub-threshold levels that arise when we put the model in a finite box. For cases with $V < 0$, the potential is attractive, and hence, a bound state in the infinite volume case may arise. Whether it is bound or not in the infinite volume case, there would appear a sub-threshold level for finite volumes. It was argued in Subsec. 4.1 that it may be not very clear, at first sight, if these levels tend to the threshold energy or to a bound state in the $L \to \infty$ limit. To circumvent this problem, we suggest here a method to study this volume dependence. By subtracting Eqs. (2.4) and (3.1), we can write the amplitude in the finite box as [62]:

$$\tilde{T}^{-1} = T^{-1} - \delta G_L, \qquad \delta G_L = \lim_{\Lambda \to \infty} \delta G = \lim_{\Lambda \to \infty} \left(\tilde{G} - G \right) . \tag{4.13}$$

A bound state with mass E_B appears as a pole in the T-matrix, thus in the vicinity of the pole, we can approximate:

$$T(E \simeq E_B) = \frac{g^2}{E - E_B} + \dots , \tag{4.14}$$

where the ellipsis denote regular terms in the Laurent series of the amplitude. The coupling can also be calculated analytically,

$$g^2 = \lim_{E \to E_B} (E - E_B) T(E) \quad \text{or} \quad \frac{1}{g^2} = \left. \frac{\mathrm{d} T^{-1}(E)}{\mathrm{d} E} \right|_{E = E_B} . \tag{4.15}$$

The volume dependence of the sub-threshold level in the finite box, given by the equation $\tilde{T}^{-1}(E) = 0$ is then dominated by this bound state, and hence:

$$\tilde{T}^{-1}(E) \simeq \frac{E - E_B}{g^2} - \delta G_L(E) = 0 , \tag{4.16}$$

13

from where one can write:

$$E(L) = E_B + g^2 \delta G_L \left[E(L), L \right] \; . \tag{4.17}$$

This equation is a reformulation of a similar result obtained in Refs. [4–6].[12] The coupling g obtained here is related to Z_ψ of Ref. [6]. Note, however, that Eq. (4.17) is appropriate as long as Eq. (4.14) is sufficiently accurate to describe the infinite volume $T-$matrix for the energy levels found in the lattice simulation (i.e., energies for which $\tilde{T}^{-1}$ vanishes). Hence, the larger the box sizes, the better Eq. (4.17) will perform.[13] We extract the mass and the coupling of the bound state from a fit to the sub-threshold level in Fig. 3 with the following χ^2 function,

$$\chi^2 = \sum_{i=1}^{5} \frac{\left(E(L_i) - E_i^{(0)} \right)^2}{\left(\Delta E_i^{(0)} \right)^2} \tag{4.18}$$

where $E(L)$ is given by Eq. (4.17).[14] The best χ^2 is $\chi^2_{\min} = 0.5$, and the parameters so obtained are:

$$E_B = 3712 \pm 6 \text{ MeV} \;, \qquad g^2 = (2.8 \pm 2.1) \text{ GeV}^{-1} \;, \tag{4.19}$$

to be compared with those obtained with the model in the infinite volume case, $E_B = 3715$ MeV and $g^2 = 2.6$ GeV^{-1}.

It could be that, for the case of weakly bound states, the error bars on the energies overlap with the threshold and it is difficult to determine if one has a bound state or not. A weak attractive potential that does not bind in the infinite volume case, still provides a level below threshold for finite volumes, and the energies go to threshold as $L \to \infty$. For this case we proceed as follows. The volume dependence of this level would be given by:

$$\tilde{T}^{-1} = 0 = T^{-1} - \delta G_L = -\frac{\mu}{2\pi} \left(-\frac{1}{a} + \frac{r}{2} k^2 + \cdots \right) - \frac{2\mu}{L^3} \frac{1}{k^2} - \alpha - \beta k^2 + \cdots$$
$$= -\frac{2\mu}{L^3 k^2} + \frac{\mu}{2\pi a} - \alpha + \left(-\frac{\mu r}{4\pi} - \beta \right) k^2 + \cdots$$

with some coefficients α and β, disregarding exponentially suppressed terms. In the above equation, we have explicitly separated the threshold singularity of δG_L,

$$\frac{1}{L^3} \frac{1}{E - m_1 - m_2} = \frac{2\mu}{L^3 k^2} \; .$$

---

[12]In the same line as in those references, but using boosted reference frames, in Ref. [63] linear combinations of energy levels are suggested to reduce the volume dependence. Our method does not rely upon the analytical form of the volume dependence to make extrapolations since for every L considered, the exact L dependence is provided by $\delta G_L(E(L), L)$.

[13]On the other hand, for very small binding energies, some subtleties appear, because the coupling g^2 tends to zero as the mass of the bound state approaches the threshold [53,64,65]. We will discuss this issue at length in Subsec. 4.6.

[14]It is worth noting the following technical detail. In principle, $E(L)$ should be extracted for each L_i as the implicit solution in Eq. (4.17) for given E_B and g^2. For practical purposes, though, it is more convenient to obtain $E(L)$ by plugging into the right-hand side of this equation the values of $E_i^{(0)}$ and L_i that we are fitting to. If Eq. (4.14) is accurate enough, both methods are equivalent, as long as the effects in Eq. (4.17) of the statistical fluctuations of the measured lattice levels are sufficiently small. In that case, the results for E_B and g^2 should not be very different, as we have checked. Indeed, the best fit results given in Eq. (4.19) have been obtained within this approximation. However, this approximation cannot be safely used when the bound state is placed close to threshold, because then δG_L rapidly changes and statistical fluctuations in the determined lattice energy levels induce large variations in the right-hand side of Eq. (4.17).

Hence, the general behavior of this level would be:

$$k^2 = \frac{2\mu}{L^3} \frac{1}{A + Bk^2} \ .$$
(4.20)

Now, this expression could be used in a χ^2 function as in Eq. (4.18) (with $k^2 < 0$ for the level below threshold). We have checked that, if we try to fit the energies of the lower level of Fig. 3 with this formula, we get a much worse χ^2 value, discarding the possibility that there is not a bound state in the infinite volume.

We have seen then that the method outlined in this subsection allows for a safe discrimination between those levels that correspond to bound states in the infinite volume and those that do not, and it also gives a precise determination of the mass. It is also worth noting that the errors for the mass of the bound state are similar to those obtained with the analysis from a potential in Subsec. 4.3, and smaller than those calculated with the phase shift analysis in Subsec. 4.2.

4.6 The case of the $I = 0$ $J^{PC} = 2^{++}$ channel

We now repeat the same analyses carried out above but now for the case of the bound state present in the $I = 0$ $J^{PC} = 2^{++}$ $D^*\bar{D}^*$ channel. As already mentioned, the 2^{++} state is a HQSS partner of the $X(3872)$ molecule which dynamics, at LO in the heavy quark expansion, is being determined by precisely the same combination of counter-terms that appear in the $X(3872)$ channel. The existence of the 2^{++} state, either as a bound state or a resonance, is a quite robust consequence of HQSS [34, 35], and it can be certainly subject to experimental detection. It is also worth to discuss this channel in this context because, contrary to the case analyzed before, we have here a very weakly bound state. In the calculation of Ref. [35], and also in the results of Subsec. 4.1, shown in the left panel of Fig. 1, charged and neutral coupled channels were studied, because the gap between both thresholds is indeed larger than the binding energy of the bound state. The mass of the bound state is $E_B = 4013.2$ MeV, whereas the neutral and charged thresholds are located at 4014.0 MeV and 4020.6 MeV, respectively. Here, however, in order to discuss the problem in simpler terms, we will consider only an uncoupled channel problem with $I = 0$, and use isospin average masses, keeping the relevant counter-term, C_0 in the nomenclature of Ref. [35], to the same value, namely, $C_0 = -0.731$ fm^2. In this way, the threshold is located at 4017.3 MeV, whereas the mass of the bound state now becomes $E_B = 4014.6$ MeV. The first two energy levels obtained with this simplified model are shown with (red) solid lines in Fig. 7. As before, for the following statistical analyses we consider the synthetic levels shown in this figure with points. The centroid of these points is randomly shifted in the range ± 5 MeV, and they are given an error of ± 10 MeV. With the points of the upper level, we generate the phase shifts shown in Fig. 8 with points, through Eq. (3.5). We can now obtain the scattering length and effective range as in Subsec. 4.2, that turn out to be:

$$\frac{1}{a} = 0.41 \pm 0.30 \text{ fm}^{-1} \ , \quad r = 0.67 \pm 0.19 \text{ fm} \ ,$$
(4.21)

with a linear Gaussian correlation $R = 0.81$. From the above fitted value for $1/a$, we find:

$$a = 2.4^{+2.4}_{-1.2} \text{ fm (68\% CL)} \ ,$$
(4.22)

while the theoretical values, obtained from Eqs.(2.9) and (2.10), are:

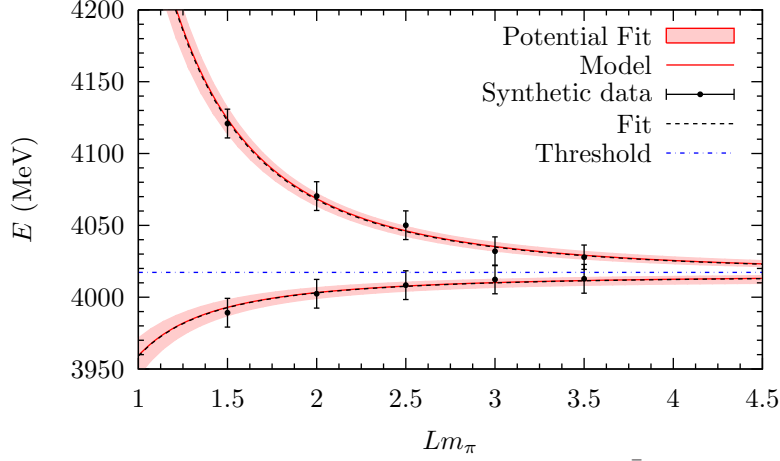$$a_{\text{th}} = 3.0 \text{ fm} \ , \quad r_{\text{th}} = 0.58 \text{ fm} \ ,$$
(4.23)

15

Figure 7: Same as in Fig. 3, but for the $I = 0$ 2^{++} $D^* \bar{D}^*$ interaction.
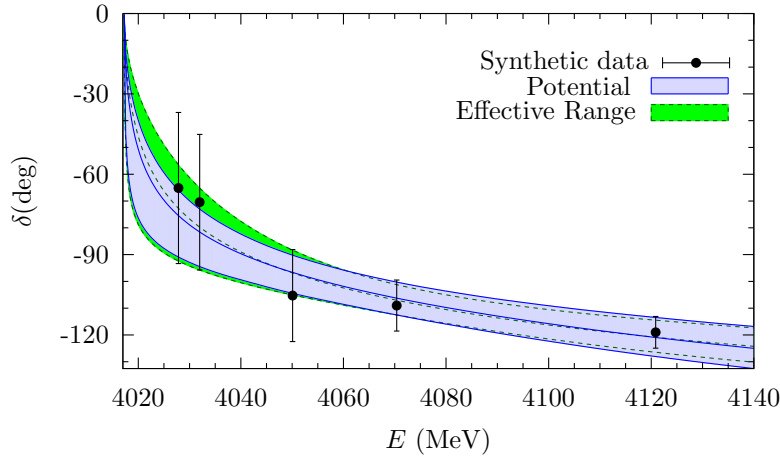

Figure 8: Phase shifts for the $I = 0$ $J^{PC} = 2^{++}$ $D^* \bar{D}^*$ channel interaction. The points stand for the synthetic phase shifts generated from the upper energy level of Fig. 7. The (green) dashed line correspond to the effective range fit, while the (blue) solid line correspond to the potential fit. The associated error bands are obtained by considering randomly chosen pair of parameters $[(1/a, r)$ and $(1/C_0, \Lambda)$ for the effective range and potential fits, respectively] that satisfy $\chi^2 \leqslant \chi^2_{\min} + 1$.

which agree with the above determinations, within errors. The phase shifts obtained with these parameters, and the associated error bands, are shown in Fig. 8 with (green) dashed lines, and they satisfactorily reproduce the synthetic data. The mass of the bound state turns out to be then $E_B = 4013^{+4}_{-18}$ MeV. Recall that the caveats raised in Subsec. 4.2 apply here.

The next step is to consider a potential fit, as in Subsec. 4.3, where the free parameters are C_0 and Λ. From a best fit, as described in Subsec. 4.3, we find:

$$\frac{1}{C_0} = -1.4 \pm 0.5 \text{ fm}^{-2} , \quad \Lambda = 1020 \pm 240 \text{ MeV} , \tag{4.24}$$

with a linear Gaussian correlation coefficient $R = -0.97$. The non-symmetrical errors given by the condition $\chi^2 \leqslant \chi^2_{\min} + 1$ are instead:

$$\frac{1}{C_0} = -1.4^{+0.4}_{-0.7} \text{ fm}^{-2} , \quad \Lambda = 1020^{+360}_{-190} \text{ MeV} . \tag{4.25}$$

The energy levels obtained with these parameters are shown in Fig. 7 with a (black) dashed line, although they are so similar to those of the exact model that they mostly overlap. Also shown in the figure are the error bands generated from the errors of the parameters, as described

previously in Fig. 3. With this potential, we can also calculate the phase shifts, which are shown in Fig. 8 with (blue) solid lines, and also the associated error band. The quality of both descriptions, that of the effective range and that of the potential, are very similar, and indeed both lines are very similar to the one of the exact model, and hence we do not show the latter. The value of C_0 deduced from Eq. (4.24) is $C_0 = -0.71^{+0.19}_{-0.39}$ fm^2 (68% CL), in good agreement with the one of the infinite volume model, $C_0 = -0.73$. Finally, the mass of the bound state is given by $E_B = 4014.3^{+2.3}_{-5.4}$ MeV. We must stress again that the errors obtained with this method are smaller than those obtained with the phase shifts analysis.

Now, we consider the method of Subsec. 4.4, in which the effective range expansion is used to study the levels below and above threshold. In this case, the best fit values that we obtain for the scattering length and effective range parameters are:

$$\frac{1}{a} = 0.35 \pm 0.15 \text{ fm}^{-1} , \qquad r = 0.64 \pm 0.15 \text{ fm} , \qquad (4.26)$$

with a linear Gaussian correlation coefficient $R = 0.3$. The non-symmetric errors stemming from the condition $\chi^2 \leqslant \chi^2_{\min} + 1$ turn out to be:

$$\frac{1}{a} = 0.35^{+0.13}_{-0.21} \text{ fm}^{-1} , \qquad r = 0.64^{+0.14}_{-0.16} \text{ fm} . \qquad (4.27)$$

Propagating the correlated Gaussian errors of Eq. (4.26), we find:

$$a = 2.9^{+2.0}_{-0.9} \text{ fm} . \qquad (4.28)$$

We note that here, as it also occurred for the $I = 0$, $J^{PC} = 2^{++}$ case, the central values obtained with this method agree better with the theoretical ones, Eq. (4.23), than those obtained with the phase shift description, Eq. (4.21), and have smaller errors than the latter ones. The mass of the bound state obtained is $E_B = 4014.2^{+2.3}_{-4.8}$ MeV, which is better determined than that obtained by means of the phase shifts analysis, and very similar to the one obtained with the potential method.

Finally, we should proceed now with the analysis performed in Subsec. 4.5. However, there is a major difference in this case, namely, that the bound state is very close to the threshold in this case. It is known that, in this case, the coupling of the state tends to zero [53, 64, 65], and so additional terms in the Laurent series, Eq. (4.14), are relevant for energies not very far from the bound state mass.[15] Further, since we are considering an error of ± 10 MeV in the energy levels, and we are trying to reproduce a bound state of binding energy of $2 - 3$ MeV, we should expect a greater qualitative impact on the lower energy levels, which are the only ones considered in this method (note that the other methods examined above use always the upper levels as well). These considerations explain why, when performing such analysis, we obtain very bad results for the bound state mass and the coupling. Hence, we must conclude that this method can only be applied safely in the case of bound states that are not very loosely bound. On the other hand, including a background term would increase the number of free parameters, and so, the errors stemming from a best fit would be even larger. At this stage, the approaches in Subsecs. 4.2 to 4.4 would be more useful for cases like this one, in which the bound state is very close to threshold.

---

[15] As an example, consider a background term in the amplitude in Eq. (4.14), so that $T = g^2/(E-E_B)+\beta+\cdots$. From the theoretical model, one can calculate $g^2 = 0.58\cdot 10^{-3}$ MeV^{-1} and $\beta = -0.68\cdot 10^{-4}$ MeV^{-2}. For energies $E \simeq 3990$ MeV, as we find for the lower level in Fig. 7 for $Lm_\pi = 1.5$, we have $\left|g^2/(E - E_B)\right| < |\beta|$.

5 Conclusions

In this paper we have addressed the interaction of heavy charmed mesons in the hidden charm sector where several bound states are produced using an interaction that is based on heavy quark spin symmetry. The interaction is then studied in a finite box and the levels expected from a lattice QCD calculation are evaluated for the $D\bar{D}$, $D^*\bar{D}^*$ states and their SU(3) partners. Then the inverse problem is faced, generating "synthetic data" from the levels obtained and using different procedures to obtain the relevant magnitudes in the infinite space, phase shifts and binding energies for the bound states. Particular emphasis is done in the error analysis to establish the accuracy of the different methods. We use two levels for different values of the box size L, one below threshold and the closest one above threshold. One strategy is to use the Lüscher formula to get phase shifts for each energy of the level above threshold. Another strategy is to use the effective range approximation, but fitting the scattering length and effective range to both levels (above and below threshold). The two methods work, but the latter one gives better determinations of the parameters (scattering length and effective range), but also of the mass of the bound state. Yet, the method that proves most efficient[16] is to parameterize a potential and a regularizing UV cutoff for the meson meson loops and carry a fit to the data. Once the potential and the UV cutoff are determined one can evaluate the phase shifts and binding energies with much better precision than the one assumed in the "synthetic data". The UV cutoff is not needed if one considers levels of only one energy, but it appears when different energies are used in the fit, yet, we show that it is highly correlated with the potential. We also devoted particular attention to the case of weakly bound states, where special care must be taken. Finally, as a byproduct we present an efficient method to obtain the Lüscher function, supported by an analytical study that allows one to truncate the sum by means of a Gaussian form factor and estimate the error induced by the truncation.

Acknowledgments

A Potentials for the $H\bar{H}$ interaction

In this Appendix, for completeness, we briefly review the formalism of the effective field theory derived in Refs. [34, 35] to study charmed meson-antimeson bound states. This effective field theory incorporates SU(3)-light flavour symmetry and HQSS. In this context and at LO, the potential is given by contact terms, related to four independent LECs, namely C_{0a}, C_{0b}, C_{1a} and C_{1b}, in the notation of Refs. [34, 35]. Thus, the potentials in the different channels will be given by different linear combinations of these LECs. The fit of these LECs to four experimental

---

[16]As one moves far away from threshold, any method based on the effective range approximation becomes less appropriated. The potential fit method improves on the effective range expansion since it includes the full loop function and not only the imaginary part fixed by unitarity. Thus, this latter method should work better when energies significantly lower or higher than the threshold are considered.

J^{PC}	$H\bar{H}'$	$^{2S+1}L_J$	V_C	J^{PC}	$H\bar{H}'$	$^{2S+1}L_J$	V_C
0^{++}	$D\bar{D}$	$^1S_0$	C_{0a}	0^+	$D\bar{D}_s$	$^1S_0$	C_{1a}
1^{++}	$D^*\bar{D}$	$^3S_1$	Eq. (A.1)	1^+	$D_s^*\bar{D}, D^*\bar{D}_s$	$^3S_1$	Eq. (A.2)
1^{+-}	$D^*\bar{D}$	$^3S_1$	$C_{0a} - C_{0b}$				
0^{++}	$D^*\bar{D}^*$	$^1S_0$	$C_{0a} - 2\,C_{0b}$	0^+	$D^*\bar{D}_s^*$	$^1S_0$	$C_{1a} - 2\,C_{1b}$
1^{+-}	$D^*\bar{D}^*$	$^3S_1$	$C_{0a} - C_{0b}$	1^+	$D^*\bar{D}_s^*$	$^3S_1$	$C_{1a} - C_{1b}$
2^{++}	$D^*\bar{D}^*$	$^5S_2$	Eq. (A.1)	2^+	$D^*\bar{D}_s^*$	$^5S_2$	$C_{1a} + C_{1b}$

Table 1: Potentials for the $H\bar{H}'$ interaction for the $I = 0$ (left) and $I = 1/2$ (right) different J^{PC} channels.

J^{PC}	$H\bar{H}'$	$^{2S+1}L_J$	V_C	J^{PC}	$H\bar{H}'$	$^{2S+1}L_J$	V_C
0^{++}	$D\bar{D}$	$^1S_0$	C_{1a}	0^{++}	$D_s\bar{D}_s$	$^1S_0$	C_{01a}
1^{++}	$D^*\bar{D}$	$^3S_1$	Eq. (A.1)	1^{++}	$D_s^*\bar{D}_s$	$^3S_1$	$C_{01a} + C_{01b}$
1^{+-}	$D^*\bar{D}$	$^3S_1$	$C_{1a} - C_{1b}$	1^{+-}	$D_s^*\bar{D}_s$	$^3S_1$	$C_{01a} - C_{01b}$
0^{++}	$D^*\bar{D}^*$	$^1S_0$	$C_{1a} - 2\,C_{1b}$	0^{++}	$D_s^*\bar{D}_s^*$	$^1S_0$	$C_{01a} - 2C_{01b}$
1^{+-}	$D^*\bar{D}^*$	$^3S_1$	$C_{1a} - C_{1b}$	1^{+-}	$D_s^*\bar{D}_s^*$	$^3S_1$	$C_{01a} - C_{01b}$
2^{++}	$D^*\bar{D}^*$	$^5S_2$	Eq. (A.1)	2^{++}	$D_s^*\bar{D}_s^*$	$^5S_2$	$C_{01a} + C_{01b}$

Table 2: Potentials for the $H\bar{H}'$ interaction for the $I = 1$ (left) and hidden strangeness sector (right) different J^{PC} channels.

data, as stated in Sec. 2, allows one to fix the numerical value of the different counterterms. In the following, we summarize the form of the potentials for the different I and J^{PC} channels.

In the isoscalar channel, the only involved LECs are C_{0a} and C_{0b}, and the way they appear in the different J^{PC} channels is shown in Table 1 (left panel). Potentials in the $I = 1/2$ and $I = 1$ sector are the same, except in the channel where coupled channels must be considered as discussed below. These potentials only depend on C_{1a} and C_{1b}. The explicit expressions for $I = 1/2$ are given in Table 1 (right panel), whereas those for $I = 1$ are shown in Table 2 (left panel). Finally, in the hidden strangeness sector, the four LECs appear, and the final potential is the arithmetic mean of the corresponding isoscalar and isovectorial interaction, as can be seen in Table 2 (right panel). Note that, for this table, we have defined $C_{01a} = \frac{1}{2}(C_{0a} + C_{1a})$ and $C_{01b} = \frac{1}{2}(C_{0b} + C_{1b})$.

However, coupled channels must be taken into account in two cases. The first one is that in which the mass difference of the charged and neutral channels thresholds is not negligible as compared to the binding energy of the state. The second case occurs when charge conjugation is not a good quantum number. The first scenario is important in the study of the $D\bar{D}^*$ system with $J^{PC} = 1^{++}$ and $D^*\bar{D}^*$ with $J^{PC} = 2^{++}$. In this case, the potential will be the interaction between the charged and neutral channels and will be given by the 2×2 matrix:

$$V_0 = \frac{1}{2}\begin{pmatrix} C_0 + C_1 & C_0 - C_1 \\ C_0 - C_1 & C_0 + C_1 \end{pmatrix}, \tag{A.1}$$

being $C_0 = C_{0a} + C_{0b}$ and $C_1 = C_{1a} + C_{1b}$. The second scenario where coupled channels are

important is because of the mixing between the $D_s\bar{D}^*$ and $D\bar{D}_s^*$ channels. In this case, the potential is:

$$V_1 = \begin{pmatrix} C_{1a} & -C_{1b} \\ -C_{1b} & C_{1a} \end{pmatrix} . \tag{A.2}$$

Using these combinations of counter-terms to describe the four input data, as explained in Sec. 2, the numerical values of the LECs for the two values of the cutoff considered in this work are the following:

$$C_{0a} = -3.366^{+0.024}_{-0.015}\,\text{fm}^2 \qquad (-1.024^{+0.005}_{-0.003}\,\text{fm}^2) , \tag{A.3}$$
$$C_{0b} = +1.673^{+0.012}_{-0.008}\,\text{fm}^2 \qquad (+0.293^{+0.004}_{-0.002}\,\text{fm}^2) , \tag{A.4}$$
$$C_{1a} = -1.76^{+0.29}_{-0.29}\,\text{fm}^2 \qquad (-0.684^{+0.064}_{-0.063}\,\text{fm}^2) , \tag{A.5}$$
$$C_{1b} = +1.68^{+0.15}_{-0.15}\,\text{fm}^2 \qquad (+0.311^{+0.033}_{-0.033}\,\text{fm}^2) , \tag{A.6}$$

for $\Lambda = 0.5\,\text{GeV}$ (1 GeV). These are the values used through this work. The uncertainties in the above equations account for possible HQSS violations and errors in the input used to fix the counter-terms (see a detailed discussion in Ref. [35]). For simplicity in this exploratory work, we have ignored them.

B Gaussian regulator and relation to Lüscher formula

In this Appendix, we discuss the details of Eq. (3.5) within a Gaussian regularization scheme. We also study the dependence of the function $\delta G(E)$, that appeared in Eq. (3.4), on the UV cutoff Λ. For convenience, we re-write $\delta G(E)$ as

$$
\begin{aligned}
\delta G(E;\Lambda) &= \tilde{G}(E) - G(E) \\
&= \overbrace{\frac{1}{L^3}\sum_{\vec{q}} \frac{e^{-2(\vec{q}^2-k^2)/\Lambda^2}-1}{E-m_1-m_2-\frac{\vec{q}^2}{2\mu}} - \int \frac{\mathrm{d}^3\vec{q}}{(2\pi)^3} \frac{e^{-2(\vec{q}^2-k^2)/\Lambda^2}-1}{E-m_1-m_2-\frac{\vec{q}^2}{2\mu}+i0^+}}^{\delta G_A} \\
&+ \underbrace{\frac{1}{L^3}\sum_{\vec{q}} \frac{1}{E-m_1-m_2-\frac{\vec{q}^2}{2\mu}} - \int \frac{\mathrm{d}^3\vec{q}}{(2\pi)^3} \frac{1}{E-m_1-m_2-\frac{\vec{q}^2}{2\mu}+i0^+}}_{\delta G_L}
\end{aligned} \tag{B.1}
$$

The function δG explicitly depends on the cutoff Λ, and this dependence is carried by the δG_A term. On the other hand, the term δG_L is well defined, and it is related to the Lüscher function [36] (see discussion below). In the strict $\Lambda \to \infty$ limit, only the second term survives, which justifies our approach in Sec. 3. Still, for practical purposes, the limit $\Lambda \to \infty$ can only be achieved by taking Λ large enough, and then it is necessary to study the dependence of δG with Λ. Let us note that δG_A has no poles, and hence it is exponentially suppressed with L according to the regular summation theorem [2,3]. For $k^2 > 0$, $E > m_1 + m_2$, δG_L is not exponentially suppressed for $L \to \infty$ and, in this case, δG_L clearly dominates over δG_A.

However for $k^2 < 0$, δG_L is also exponentially suppressed as L increases, and therefore one needs to explicitly calculate the dependence of δG_A on ΛL.

Let us calculate the derivative of δG with respect to Λ. Only δG_A depends on Λ, and this latter function does it through the exponential function $\exp[-2(\vec{q}^2 - k^2)/\Lambda^2]$. The derivative

brings down a factor $(\vec{q}^2 - k^2)$ that cancels out the denominators. This greatly simplifies the calculation of both the sum and the integral. The latter one is trivial and it only amounts to the integration of a Gaussian function, while the former one, up to constant factors, now reads

$$\frac{1}{L^3}\sum_{\vec{q}}e^{-2\vec{q}^2/\Lambda^2} = \left(\frac{1}{L}\sum_{n=-\infty}^{+\infty}e^{-2\left(\frac{2\pi}{L}\right)^2\frac{n^2}{\Lambda^2}}\right)^3 = \left[\frac{\theta_3(0, e^{-\frac{8\pi^2}{\Lambda^2L^2}})}{L}\right]^3 \tag{B.2}$$

where we have used $\vec{q}^2 = q_x^2 + q_y^2 + q_z^2$ and that the exponential of a sum is the product of the exponentials. This latter property allows to relate the sum in three dimensions to the cube of the sum in one dimension. In Eq. (B.2), $\theta_3(u, \alpha)$ is a Jacobi elliptic theta function [66]. It satisfies [67],

$$\frac{\theta_3(0, e^{-\pi x^2})}{\theta_3(0, e^{-\pi/x^2})} = \frac{1}{x} . \tag{B.3}$$

This allows us to write then:

$$\frac{\partial \, \delta G}{\partial \Lambda} = -\frac{\mu}{(2\pi)^{3/2}}e^{2k^2/\Lambda^2}\left(\left[\theta_3(0, e^{-\Lambda^2L^2/8})\right]^3 - 1\right) . \tag{B.4}$$

We note that this equation is exact. The above equation converges rapidly to zero as the Gaussian cutoff increases, which shows that the limit $\Lambda \to \infty$ is effectively quickly achieved. To proceed further, we note that:

$$[\theta_3(0, \alpha)]^3 = 1 + 6\alpha + 12\alpha^2 + \cdots = \sum_{m=0}^{\infty}c_m\alpha^m , \tag{B.5}$$

and the coefficients c_m are nothing but the multiplicities of $m = \vec{n}^2, \vec{n} \in \mathbb{Z}^3$. Since $\alpha = e^{-\Lambda^2L^2/8}$, we can find the leading term in Eq. (B.4),

$$\frac{\partial \, \delta G}{\partial \Lambda} = -\frac{6\mu}{(2\pi)^{3/2}}\exp\left(\frac{2k^2}{\Lambda^2} - \frac{\Lambda^2L^2}{8}\right)\left(1 + \mathcal{O}\left(e^{-\Lambda^2L^2/8}\right)\right) . \tag{B.6}$$

Given that $\delta G = \delta G_L$ for $\Lambda \to \infty$, we find keeping just the leading term:

$$\delta G(E; \Lambda) = \delta G_L(E) + \frac{6\mu}{(2\pi)^{3/2}}\int_\Lambda^\infty d\Lambda' \exp\left(\frac{2k^2}{\Lambda'^2} - \frac{\Lambda'^2L^2}{8}\right) \tag{B.7}$$

$$= \delta G_L(E) + \frac{3\mu}{2\pi L}\left[e^{ikL}\text{erfc}\left(\frac{\Lambda L}{2\sqrt{2}} + i\frac{\sqrt{2}k}{\Lambda}\right) + e^{-ikL}\text{erfc}\left(\frac{\Lambda L}{2\sqrt{2}} - i\frac{\sqrt{2}k}{\Lambda}\right)\right] ,$$

and, then, its asymptotic behavior is:

$$\delta G(E; \Lambda) = \delta G_L(E) + \frac{24\mu}{(2\pi)^{3/2}}\frac{e^{-\frac{\Lambda^2L^2}{8}}}{\Lambda L^2}\left[1 + \frac{2(k^2L^2 - 2)}{L^2\Lambda^2} + \mathcal{O}\left(\Lambda^{-4}\right)\right] + \cdots , \tag{B.8}$$

where $\mathcal{O}(\Lambda^{-4})$ refers to $(k/\Lambda)^4$, $(k^2/L^2)/\Lambda^4$ and $1/(L\Lambda)^4$, and the ellipsis stands for terms that are more exponentially suppressed (the next one would take the form $e^{-\Lambda^2L^2/4}$). Given the form of the L suppression, the Gaussian regularization scheme does not introduce any spurious terms that would dominate over[17] the physical contribution δG_L, as long as Λ is sufficiently large.

---

[17]As already mentioned, for $k^2 > 0$ δG_L is not exponentially suppressed for $L \to \infty$, while for $k^2 < 0$, we expect δG_L to decrease as $\exp(-|k|L)$.

Indeed, one can efficiently compute the regularized Lüscher function by means of the Gaussian regulated δG loop function. The Lüscher function[18] is related to the loop functions by means of [36]:

$$\sqrt{4\pi}\mathcal{Z}_{00}(1,\hat{k}^2) = -\frac{L}{2\pi}\frac{(2\pi)^3}{2\mu}\delta G_L(E), \quad \hat{k}^2 = \frac{k^2 L^2}{(2\pi)^2} \; . \tag{B.9}$$

Thus, for a mildly large value of Λ, $\delta G_L(E)$ can be approximated by the Gaussian regulated $\delta G(E, \Lambda)$ function, up to corrections suppressed by the exponential factor $e^{-\frac{\Lambda^2 L^2}{8}}$ (see Eq. (B.8)),

$$\sqrt{4\pi}\mathcal{Z}_{00}(1,\hat{k}^2) = -\frac{L}{2\pi}\frac{(2\pi)^3}{2\mu}\left(\delta G(E,\Lambda) + \mathcal{O}\left(e^{-\frac{\Lambda^2 L^2}{8}}\right)\right) \tag{B.10}$$

which in turn provides $\mathcal{Z}_{00}(1,\hat{k}^2)$ with enough accuracy in a computationally easy way.

C Cutoff effects and relation to dispersion relations

In this Appendix and to better frame the approach followed in Subsec. 4.3, the existing correlation between the constant of the potential and the cutoff is addressed in detail. We also discuss the relation of our approach to other approaches in which the loop function is calculated from a dispersion relation.

We recall Eqs. (2.5) and (2.7) to expand the inverse of the amplitude in powers of k^2. For more general purposes, we consider a potential in which the factor that multiplies the Gaussian, $\exp\left(-2k^2/\Lambda^2\right)$, has some energy dependence instead of being constant. It is to say, we replace in Eq. (2.7) C by $C(E) = c_1 + c_2 k^2$, that reduces to the original form by setting $c_2 = 0$. We find

$$V^{-1} - G = \frac{1}{c_1} + \frac{\mu\Lambda}{(2\pi)^{3/2}} + \left(-\frac{c_2}{c_1^2} + \frac{2}{c_1\Lambda^2} - \frac{2\mu}{(2\pi)^{3/2}\Lambda}\right)k^2 + i\frac{\mu k}{2\pi} + \mathcal{O}(k^4) \; . \tag{C.1}$$

For model-given values of c_1 and c_2 for an imposed cutoff Λ, one can shift the cutoff to Λ' and have the same T-matrix, up to $\mathcal{O}(k^4)$, by reabsorbing the cutoff shift in the new parameters c_1' and c_2', given by:

$$\frac{1}{c_1'} = \frac{1}{c_1} + \frac{\mu(\Lambda - \Lambda')}{(2\pi)^{3/2}} \; , \tag{C.2}$$

$$\frac{c_2'}{c_1'^2} = \frac{c_2}{c_1^2} + \frac{2}{c_1}\frac{\Lambda^2 - \Lambda'^2}{\Lambda^2\Lambda'^2} + \frac{2\mu(\Lambda - \Lambda')^2}{(2\pi)^{3/2}\Lambda\Lambda'^2} \; . \tag{C.3}$$

If we insist in a constant potential, $c_2 = c_2' = 0$, we can also reabsorb the cutoff effects in c_1, but this would be correct just up to $\mathcal{O}(k^2)$.

Let us consider an approach in which the amplitude is written with a loop function regu-

---
[18]It satisfies [3],

$$e^{2i\delta} = \frac{k\cot\delta + ik}{k\cot\delta - ik} = \frac{\mathcal{Z}_{00}(1,\hat{k}^2) + i\pi^{\frac{3}{2}}\hat{k}}{\mathcal{Z}_{00}(1,\hat{k}^2) - i\pi^{\frac{3}{2}}\hat{k}}.$$

larized by means of a once–subtracted dispersion relation (DR),[19]

$$T_{\mathrm{DR}}^{-1} = V_{\mathrm{DR}}^{-1} - G_{\mathrm{DR}} \; , \tag{C.4}$$

$$V_{\mathrm{DR}} = C \; , \tag{C.5}$$

$$G_{\mathrm{DR}} = \alpha - i\frac{\mu k}{2\pi} \; , \tag{C.6}$$

where C is the potential, analogous to the case of the Gaussian regulator approach, and α is a subtraction constant (a free parameter of the approach). Considering, as before, $C = c_1 + c_2 k^2$, we can expand:

$$V_{\mathrm{DR}}^{-1} - G_{\mathrm{DR}} = \frac{1}{c_1} - \alpha - \frac{c_2}{c_1^2}k^2 + i\frac{\mu k}{2\pi} + \mathcal{O}(k^4) \; . \tag{C.7}$$

We can then reabsorb the effects up to $\mathcal{O}(k^4)$ of an arbitrary shift in the subtraction constant by means of:

$$\frac{1}{c_1'} = \frac{1}{c_1} + \alpha' - \alpha \; , \tag{C.8}$$

$$c_2' = \frac{c_1'^2}{c_1^2}c_2 \; . \tag{C.9}$$

We see that the effects of the shift can be reabsorbed *exactly* for a constant potential, with the first of the previous equations. However, in the more general case of energy dependent potentials (as the case of chiral potentials, for example), this cannot be made exactly but just up to $\mathcal{O}(k^4)$. We see thus that there are several equivalent ways: one can fit, in the Gaussian regulator case, a constant for the potential and the cutoff, or fix the latter to a reasonable (but otherwise arbitrary) value and fit two constants. In a dispersion relation, a similar situation is found, where now the subtraction constant plays the equivalent role of the cutoff. In Subsec. 4.3 we have followed the first approach. In Fig. 5, we show, for the case of $I = 0$ $J^{PC} = 0^{++}$ $D\bar{D}$, the contours curves of the χ^2 function in terms of the free parameters: the UV cutoff Λ and the inverse of the constant (C_{0a}) that appears in the potential for this channel. We see already from this figure that Λ and $1/C_{0a}$ are strongly correlated, and that the correlation is of the form given in Eq. (C.2). Indeed, the dashed line in the plot, that lies close to the axis of the error ellipse, is Eq. (C.2) using the central values of the cutoff and the potential given in the original work of Ref. [35], $\Lambda = 1000$ MeV and $C_{0a} = -1.024$ fm^2. We also infer that the correlation is stronger for higher values of the cutoff, since the quadratic terms in Eq. (C.1) become less important as Λ increases.

References

[1] Z. Fodor and C. Hoelbling, Rev. Mod. Phys. **84**, 449 (2012).

[2] M. Lüscher, Commun. Math. Phys. **105**, 153 (1986).

[3] M. Lüscher, Nucl. Phys. B **354**, 531 (1991).

[4] M. Luscher, Commun. Math. Phys. **104**, 177 (1986).

---

[19]The expression for the loop function can be found by applying the dispersion relation integral, or, in a more handy way, by taking the limit $\Lambda \to \infty$ for the case of the Gaussian regulator loop integral and reabsorbing the infinity in the subtraction constant.

[5] S. R. Beane, P. F. Bedaque, A. Parreno and M. J. Savage, Phys. Lett. B **585**, 106 (2004).

[6] S. R. Beane *et al.* [NPLQCD Collaboration], Phys. Rev. D **85**, 054511 (2012).

[7] X. Feng *et al.* [ETM Collaboration], PoS LAT **2010**, 104 (2010).

[8] S. Aoki *et al.* [CP-PACS Collaboration], Phys. Rev. D **76**, 094506 (2007).

[9] M. Gockeler *et al.* [QCDSF Collaboration], PoS LATTICE **2008**, 136 (2008).

[10] S. Aoki *et al.* [PACS-CS Collaboration], PoS LATTICE **2010**, 108 (2010).

[11] X. Feng, K. Jansen and D. B. Renner, Phys. Rev. D **83**, 094505 (2011).

[12] J. Frison *et al.* [BMW Collaboration], PoS LATTICE **2010**, 139 (2010).

[13] C. B. Lang, D. Mohler, S. Prelovsek and M. Vidmar, Phys. Rev. D **84**, 054503 (2011).

[14] S. Prelovsek, C. B. Lang, D. Mohler and M. Vidmar, PoS LATTICE **2011**, 137 (2011).

[15] J. J. Dudek, R. G. Edwards and C. E. Thomas, Phys. Rev. D **87**, 034505 (2013).

[16] L. Roca and E. Oset, Phys. Rev. D **85**, 054507 (2012).

[17] S. Prelovsek, T. Draper, C. B. Lang, M. Limmer, K. -F. Liu, N. Mathur and D. Mohler, Phys. Rev. D **82**, 094507 (2010).

[18] C. Alexandrou, J. O. Daldrop, M. D. Brida, M. Gravina, L. Scorzato, C. Urbach and M. Wagner, arXiv:1212.1418 [hep-lat].

[19] Z. Fu, JHEP **1207**, 142 (2012).

[20] Z. Fu, arXiv:1303.0517 [hep-lat].

[21] D. Mohler and R. M. Woloshyn, Phys. Rev. D **84**, 054505 (2011).

[22] M. Kalinowski and M. Wagner, arXiv:1212.0403 [hep-lat].

[23] D. Mohler, S. Prelovsek and R. M. Woloshyn, arXiv:1208.4059 [hep-lat].

[24] S. Ozaki and S. Sasaki, PoS LATTICE **2012**, 160 (2012).

[25] T. Kawanai and S. Sasaki, PoS LATTICE **2010**, 156 (2010).

[26] Y. -B. Yang, Y. Chen, L. -C. Gui, C. Liu, Y. -B. Liu, Z. Liu, J. -P. Ma and J. -B. Zhang, arXiv:1206.2086 [hep-lat].

[27] L. Liu, K. Orginos, F. -K. Guo, C. Hanhart and U. -G. Meissner, Phys. Rev. D **87**, 014508 (2013).

[28] A. Martinez Torres, L. R. Dai, C. Koren, D. Jido and E. Oset, Phys. Rev. D **85**, 014027 (2012).

[29] J. -J. Xie and E. Oset, Eur. Phys. J. A **48**, 146 (2012).

[30] J. M. Flynn and J. Nieves, Phys. Rev. D **75**, 074024 (2007).

[31] D. Gamermann, E. Oset, D. Strottman and M. J. Vicente Vacas, Phys. Rev. D **76**, 074016 (2007).

[32] D. Gamermann and E. Oset, Eur. Phys. J. A **36**, 189 (2008).

[33] P. Pakhlov *et al.* [Belle Collaboration], Phys. Rev. Lett. **100**, 202001 (2008).

[34] J. Nieves and M. P. Valderrama, Phys. Rev. D **86**, 056004 (2012).

[35] C. Hidalgo-Duque, J. Nieves and M. P. Valderrama, arXiv:1210.5431 [hep-ph].

[36] M. Doring, U. -G. Meißner, E. Oset and A. Rusetsky, Eur. Phys. J. A **47**, 139 (2011).

[37] J. A. Oller, E. Oset and A. Ramos, Prog. Part. Nucl. Phys. **45**, 157 (2000).

[38] J. Nieves and E. Ruiz Arriola, Phys. Lett. B **455**, 30 (1999).

[39] J. Nieves and E. Ruiz Arriola, Nucl. Phys. A **679**, 57 (2000).

[40] J. A. Oller and U. G. Meissner, Phys. Lett. B **500**, 263 (2001).

[41] T. Hyodo, S. I. Nam, D. Jido and A. Hosaka, Phys. Rev. C **68**, 018201 (2003).

[42] C. Garcia-Recio, M. F. M. Lutz and J. Nieves, Phys. Lett. B **582**, 49 (2004).

[43] M. Doring, J. Haidenbauer, U. -G. Meißner and A. Rusetsky, Eur. Phys. J. A **47**, 163 (2011).

[44] M. Doring and U. G. Meißner, JHEP **1201**, 009 (2012).

[45] H. -X. Chen and E. Oset, Phys. Rev. D **87**, 016014 (2013).

[46] A. Martinez Torres, M. Bayar, D. Jido and E. Oset, Phys. Rev. C **86**, 055201 (2012).

[47] M. Albaladejo, J. A. Oller, E. Oset, G. Rios, and L. Roca, JHEP **1208**, 071 (2012).

[48] F. Aceti, R. Molina and E. Oset, Phys. Rev. D **86**, 113007 (2012).

[49] M. P. Valderrama, Phys. Rev. D **85**, 114037 (2012).

[50] G.F. Chew and S. Mandelstam, Phys. Rev. **119**, 467 (1960).

[51] J. A. Oller and E. Oset, Phys. Rev. D **60**, 074023 (1999).

[52] M. Albaladejo and J. A. Oller, Phys. Rev. Lett. **101**, 252002 (2008).

[53] M. Albaladejo and J. A. Oller, Phys. Rev. D **86**, 034003 (2012).

[54] J. M. M. Hall, A. C. -P. Hsu, D. B. Leinweber, A. W. Thomas and R. D. Young, arXiv:1303.4157 [hep-lat].

[55] G. P. Lepage, arXiv:hep-ph/0506330.

[56] G. P. Lepage, arXiv:nucl-th/9706029.

[57] E. Epelbaum and U.-G. Meißner, arXiv:nucl-th/0609037.

[58] E. Epelbaum and J. Gegelia, Eur. Phys. J. A **41**, 341 (2009).

[59] S. K. Choi *et al.* [Belle Collaboration], Phys. Rev. Lett. **91**, 262001 (2003).

[60] A. Tomaradze, S. Dobbs, T. Xiao, K. K. Seth and G. Bonvicini, arXiv:1212.4191 [hep-ex].

[61] R. Molina and E. Oset, Phys. Rev. D **80**, 114013 (2009).

[62] E. Oset, Eur. Phys. J. A **49**, 32 (2013).

[63] Z. Davoudi and M. J. Savage, Phys. Rev. D **84**, 114502 (2011).

[64] H. Toki, C. Garcia-Recio and J. Nieves, Phys. Rev. D **77**, 034001 (2008).

[65] D. Gamermann, J. Nieves, E. Oset and E. Ruiz Arriola, Phys. Rev. D **81**, 014029 (2010).

[66] E. T. Whittaker and G. N. Watson, *A Course in Modern Analysis*, 4th ed. Cambridge, England: Cambridge University Press, 1990.

[67] H. M. Edwards, *Riemann's Zeta Function*, New York: Dover, 2001.